# Development and application of a comprehensive measurement equation for the direct comparator standardization method of Instrumental Neutron Activation Analysis

Spectrochimica Acta Part B: Atomic Spectroscopy 218 (2024) 106997

Contents lists available at ScienceDirect

Spectrochimica Acta Part B: Atomic Spectroscopy

journal homepage: www.elsevier.com/locate/sab

# Development and application of a comprehensive measurement equation for the direct comparator standardization method of Instrumental Neutron Activation Analysis

Giancarlo D'Agostino *, Marco Di Luzio

*Istituto Nazionale di Ricerca Metrologica (INRIM), Unit of Radiochemistry and Spectroscopy c/o Department of Chemistry, University of Pavia, via Taramelli 12, 27100 Pavia, Italy*

ARTICLE INFO

*Keywords:*
Instrumental Neutron Activation Analysis
Measurement equation
Primary ratio method
Inorganic chemistry
Uncertainty budget

ABSTRACT

A comprehensive model equation for the measurement of elemental mass fractions in solid materials using the direct standardization method of Instrumental Neutron Activation Analysis was developed. The extensive modelling established for the single comparator standardization was revised and changed for the direct standardization to obtain a complete mathematical description of the measurand by physical and chemical quantities having dimensions in SI units. The model equation is presented both in case measurement and standard samples are measured in the same γ-counting position and in different γ-counting positions. The first was successfully applied for the quantitative determination of As mass fraction in a seafood matrix with a percent level relative uncertainty. The SI traceability of the result is established by a traceable standard via the measurement equation and the uncertainty budget compiled to highlight the input quantities that contribute most to the combined uncertainty.

## 1. Introduction

In 2007, the Consultative Committee for Amount of Substance: Metrology in Chemistry and Biology (CCQM) has acknowledged the direct comparator standardization method of Instrumental Neutron Activation Analysis (INAA), hereafter called rel-INAA method, fulfilling the definition of a primary ratio method [1–3].

The basis for recognition is that the operation of the rel-INAA method can be completely described by a measurement equation linking the amount of substance value to measured quantities that can be expressed in terms of SI units, as well as their uncertainties. Accordingly, the method has the potential to establish the first link in the chain of traceability to SI for amount of substance values of specified major, minor or trace chemical elements in complex matrix reference materials [4].

Fundamental principles and metrological characteristics of NAA have been recalled in a review published in 2011 by Greenberg et al. [5] which also includes the measurement equation adopted to obtain the acknowledgement of rel-INAA as a potential primary ratio method. Based on this equation, a list consisting of 30 uncertainty components divided into three groups depending on the operation stage, i.e. (i) pre-irradiation, (ii) irradiation and (iii) γ-ray spectrometry, is reported and discussed.

Although all sources contributing to the uncertainty are discussed in fine details, their modelling by input quantities in the measurement equation is limited. This is the case of (i) neutron self-shielding and flux gradient, (ii) neutron energy spectrum, and (iii) γ-ray self-absorption, counting position and geometry which are grouped in (i) neutron fluences, (ii) effective cross sections and (iii) counting efficiencies ratios, respectively. As a result, the actual use of the proposed measurement equation required further developments.

Aiming at a general improving of the modelling available for the direct comparator standardization method, we revised the measurement equation developed for the single comparator standardization method [6] of INAA, called $k_0$-INAA, to exploit the possibility of using it for the rel-INAA method when the comparator element corresponds to the element of interest, hereafter called analyte.

Nowadays, the $k_0$-INAA method is used at the highest metrological levels in CCQM key-comparisons of mass fraction determination of trace elements in complex matrices [7]. The use of the comparator element, also called monitor, to quantify any analyte via the corresponding $k_0$-value, required a lot of effort in modelling fundamental principles of

* Corresponding author.
*E-mail addresses:* g.dagostino@inrim.it (G. D'Agostino), m.diluzio@inrim.it (M. Di Luzio).

https://doi.org/10.1016/j.sab.2024.106997
Received 5 February 2024; Received in revised form 9 May 2024; Accepted 12 July 2024
Available online 14 July 2024

neutron activation and γ-ray counting. The method was firstly proposed by Simonits et al. in 1975 [8] and later extensively developed by De Corte [9] to take full advantage of the multi-elemental features of INAA.

In this paper, we present the development of a comprehensive measurement equation for the rel-INAA method implementing the detailed modelling adopted in the $k_0$-INAA method. Results obtained using the measurement equation in an experiment carried out to quantify As mass fraction in a seafood matrix within the framework of an international supplementary comparison are also given.

## 2. The measurement equation

According to the equation model developed for the $k_0$-INAA method, the mass fraction of an analyte in a cylindrical measurement sample which is co-irradiated with a monitor in a cylindrical standard sample is

$$w_{\text{smp (a)}} = \left( \left. \frac{\lambda \frac{(n_p/COI)(t_c/t_l)\, e^{\mu(1-t_l/t_c)}}{(1-e^{-\lambda\, t_l})(1-e^{-\lambda\, t_c})} \right|_{\text{smp (a)}} \Big/ \left. \frac{\lambda \frac{(n_p/COI)(t_c/t_l)\, e^{\mu(1-t_l/t_c)}}{(1-e^{-\lambda\, t_l})(1-e^{-\lambda\, t_c})} \right|_{\text{std (m)}} \right) e^{(\lambda_a-\lambda_m)\, t_{\text{d std (m)}}+\lambda_a\, \Delta t_d} \frac{1}{k_\beta} \times \frac{k_{0\ \text{Au}}(\text{m})}{k_{0\ \text{Au}}(\text{a})} \frac{G_{\text{th std (m)}} + \frac{G_{\text{e std (m)}}}{f}\, Q_{0\ \text{m}}(\alpha)}{G_{\text{th smp (a)}} + \frac{G_{\text{e smp (a)}}}{f}\, Q_{0\ \text{a}}(\alpha)} k_\varepsilon \times m_{\text{std}}\, k_{\text{buy}}\, (1-\eta_{\text{std}})\, w_{\text{std (m)}} - m_{\text{blk}}\, w_{\text{blk (a)}} \Big) \frac{1}{m_{\text{smp}}(1-\eta_{\text{smp}})} - \Delta w_U \tag{1}$$

where $w$ is the mass fraction, $m$ is the weighted mass, $\eta$ is the moisture mass to sample mass ratio, $k_{\text{buy}}$ is the air buoyancy correction factor, $\lambda = ln(2)/t_{1/2}$ is the decay constant of the radionuclide having a half-life $t_{1/2}$, $n_p$ is the number of counts in the full-energy γ-peak (net of the counts due to background and interfering γ-peaks), *COI* is the true-coincidence correction factor, $t_c$ and $t_l$ are the counting and live times of the $\gamma$-ray detection system, $\Delta t_d$ is the difference of decay times, $k_\beta$ is the analyte count rate correction due to vertical gradient of the neutron flux, $k_{0\ \text{Au}}$ is the $k_0$ factor with Au being the ultimate comparator, $G_{\text{th}}$ and $G_e$ are the thermal and epi-thermal neutron self-shielding correction factors, $\Delta w_U$ is the mass fraction correction due to radionuclides produced by U fissions in the sample, $f$ is the (conventional) sub- to *epi-* cadmium neutron flux, $\alpha$ is the *epi*-cadmium neutron shape factor, $Q_0(\alpha)$ is the ratio of the resonance integral (for a $1/E^\alpha$ neutron spectrum in the epi-cadmium energy region) to the thermal cross section and $k_\varepsilon$ is the ratio of $\gamma$-detection efficiencies. Subscripts a and m refer to analyte and monitor respectively, and smp, std and blk refer to measurement sample, standard sample and blank, respectively. Furthermore, subscripts smp (a) and std (m) refer to analyte and monitor in measurement and standard sample, respectively. Input quantities that are not mentioned in this work are discussed in [6,10].

It is worth noting that second order effects due to possible vertical gradients in $f$ are not modeled. In addition, in case of measurement of very short half-life radionuclides governing the count rate of the detection system, real time acquisitions algorithms are required to obtain $n_p$ values already corrected for dead dead-time. Use of the Eq. (1) is still possible by setting $t_c = t_l$.

Whether the target isotope of the monitor and analyte is the same, the $k_0$-INAA method turns into the rel-INAA method. Therefore, a rel-INAA measurement equation can be developed starting from (1). For that purpose, it is useful to explicitly write the following three terms $k_{0\ \text{Au}}$ (m), $k_{0\ \text{Au}}$ (a), $k_\varepsilon$, and $k_{\text{buy}}$:

$$k_{0\ \text{Au}}(\text{m}) = \frac{M_{\text{Au}}\, \theta_{E^i\ \text{std (m)}}\, \gamma_{\text{m}}\, \sigma_{0\ \text{m}}}{M_{\text{std (m)}}\, \theta_{\text{Au}}\, \gamma_{\text{Au}}\, \sigma_{0\ \text{Au}}} \text{ and } k_{0\ \text{Au}}(\text{a}) = \frac{M_{\text{Au}}\, \theta_{E^i\ \text{smp (a)}}\, \gamma_{\text{a}}\, \sigma_{0\ \text{a}}}{M_{\text{smp (a)}}\, \theta_{\text{Au}}\, \gamma_{\text{Au}}\, \sigma_{0\ \text{Au}}} \tag{2}$$

where $\theta_{i_E}$ is the amount fraction of the target isotope $^iE$, $M = \sum_i \theta_{i_E} M_{i_E}$ is the molar mass of the target element, $\gamma$ is the γ-ray yield of the produced and detected radionuclide and $\sigma_0$ is the thermal neutron cross section of the target isotope,

$$k_\varepsilon = k_{\varepsilon\Delta E}\, k_{\varepsilon\Delta d}\, k_{\text{pos}}\, k_{\text{geo}}\, k_{\text{sa}} \tag{3}$$

where $k_{\varepsilon\Delta E} = e^{\sum_{j=1}^{6} a_j \left(E_m^{2-j} - E_a^{2-j}\right)}$ is the monitor-to-analyte efficiency ratio of γ-rays emitted at energy $E$ at reference position, $k_{\varepsilon\Delta d}$ is the analyte reference-to-counting and monitor counting-to-reference efficiency ratios product, $k_{\text{pos}}$ and $k_{\text{geo}}$ are monitor-to-analyte efficiency correction ratios due to actual sample positioning and extended cylindrical sample geometry, respectively, and $k_{\text{sa}}$ is the monitor-to-analyte γ-ray self-absorption correction ratio; details of the modelling developed for $k_\varepsilon$ are given in [6];

$$k_{\text{buy}} = \frac{1 + \left(\frac{1}{\rho_{\text{std}}} - \frac{1}{\rho_c}\right) \rho_a}{1 + \left(\frac{1}{\rho_{\text{smp}}} - \frac{1}{\rho_c}\right) \rho_a} \tag{4}$$

where $\rho_{\text{std}}$, $\rho_{\text{smp}}$, $\rho_c$ and $\rho_a$ are densities of standard sample, measurement sample, reference weight (used to calibrate the balance) and air, respectively [11].

After replacing (2) and (3) in (1), dropping subscript a and m, simplifying and rearranging we obtain the measurement equation for the rel-INAA method:

$$w_{\text{smp}} = \left( \frac{n_{\text{p smp}}}{n_{\text{p std}}} \frac{COI_{\text{std}}}{COI_{\text{smp}}} \frac{t_{\text{c smp}}}{t_{\text{c std}}} \frac{t_{\text{l std}}}{t_{\text{l smp}}} \frac{1-e^{-\lambda\, t_{\text{c std}}}}{1-e^{-\lambda\, t_{\text{c smp}}}} e^{\mu\left(\frac{t_{\text{l std}}}{t_{\text{c std}}} - \frac{t_{\text{l smp}}}{t_{\text{c smp}}}\right)} e^{\lambda\, \Delta t_d} \frac{1}{k_\beta} \times \frac{\theta_{i_E\ \text{std}}\, M_{\text{smp}}}{\theta_{i_E\ \text{smp}}\, M_{\text{std}}} \frac{G_{\text{th std}} + \frac{G_{\text{e std}}}{f}\, Q_0(\alpha)}{G_{\text{th smp}} + \frac{G_{\text{e smp}}}{f}\, Q_0(\alpha)} k_{\varepsilon\Delta d}\, k_{\text{pos}}\, k_{\text{geo}}\, k_{\text{sa}} \times m_{\text{std}}\, k_{\text{buy}}\, (1-\eta_{\text{std}})\, w_{\text{std}} - m_{\text{blk}}\, w_{\text{blk}} \right) \frac{1}{m_{\text{smp}}(1-\eta_{\text{smp}})} - \Delta w_U \tag{5}$$

where

$$COI = \left(1 - \sum_i F_{\text{loss}}(i)\right) \left(1 + \sum_i F_{\text{sum}}(i)\right) \tag{6}$$

is obtained from a pool of functions $F_{\text{loss}}$ and $F_{\text{sum}}$ evaluating loss and summing effects caused by cascade emissions $i$ involved in a true-coincidence with the detected γ-ray. Details for calculating $F_{\text{loss}}$ and $F_{\text{sum}}$ are given in [6];

$$\Delta t_d = t_{\text{d smp}} - t_{\text{d std}} \tag{7}$$

is obtained from decay times, $t_d$, calculated from the neutron irradiation end to the γ-ray counting start;

$$k_\beta = 1 + \beta \Delta l \tag{8}$$

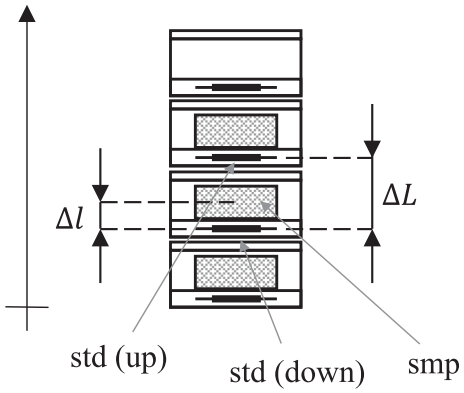


**Fig. 1.** Position of the measurement (smp) and standard (std) samples within the irradiation container.

is obtained from the vertical count rate gradient per unit distance, $\beta$, and the distance between center of mass of the measurement sample and standard sample within the irradiation container, $\Delta l$. To reach the best accuracy we bracket the measurement sample with two standard samples (see Fig. 1). Under the assumption of a linear gradient, we adopt the formula $\beta = \frac{\Gamma_{\text{sp std (up)}}/\Gamma_{\text{sp std (down)}}-1}{\Delta L}$, with $\Gamma_{\text{sp std (up)}}$ and $\Gamma_{\text{sp std (down)}}$ being (mass) specific γ-ray emission rates of the two standard samples and $\Delta L$ their vertical distance (the Cartesian coordinate axis originates at the bottom of the irradiation channel and is oriented upwards);

$$G_{\text{th}} = \frac{1}{1+\left(\frac{z_{\text{th}}}{z_{0\ \text{th}}}\right)^{p_{\text{th}}}} \tag{9}$$

is obtained from dimensionless variables $p_{\text{th}}$, $z_{0\ \text{th}}$ and $z_{\text{th}}$, according to thermal neutron self-shielding modelling proposed by Martinho et al. [12] occurring in a cylindrical sample with mass $m_{\text{smp}}$, radius $r$, height $h$, and composed of a number of elements $E_j$ with mass fraction $w_{E_j}$ having thermal absorption and scattering cross sections $\sigma_{\text{ab}\ E_j} = \sum_i \theta_{i_{E_j}} \sigma_{\text{ab}\ i_{E_j}}$ and $\sigma_{\text{sc}\ E_j} = \sum_i \theta_{i_{E_j}} \sigma_{\text{sc}\ i_{E_j}}$, respectively. Specifically, $p_{\text{th}} = 1.061(4)$, $z_{0\ \text{th}} = 0.635(2)$ and $z_{\text{th}} = \frac{m_{\text{smp}} N_A}{\pi r (r+h)} \sum_j \frac{w_{E_j} \sigma_{\text{T}\ E_j}}{M_j} \left(\frac{\sigma_{\text{ab}\ E_j}}{\sigma_{\text{T}\ E_j}}\right)^{0.85}$, with $\sigma_{\text{T}\ E_j} = \sigma_{\text{ab}\ E_j} + \sigma_{\text{sc}\ E_j}$. Values for $\sigma_{\text{ab}\ i_{E_j}}$ and $\sigma_{\text{sc}\ i_{E_j}}$ are reported in [13]. Here and hereafter digits in parenthesis represent standard uncertainty;

$$G_{\text{e}} = \frac{A_1 - A_2}{1+\left(\frac{z_{\text{e}}}{z_{0\ \text{e}}}\right)^{p_{\text{e}}}} + A_2 \tag{10}$$

is obtained from dimensionless variables $A_1$, $A_2$, $p_{\text{e}}$, $z_{0\ \text{e}}$ and $z_{\text{e}}$, according to epithermal neutron self-shielding modelling proposed by Goncalves et al. [14] occurring in a cylindrical sample with mass $m_{\text{smp}}$, radius $r$, height $h$, and having the target analyte element as a major component. Specifically, $A_1 = 1.000(5)$, $A_2 = 0.060(11)$, $p_{\text{e}} = 0.82(2)$, $z_{0\ \text{e}} = 2.70(9)$ and $z_{\text{e}} = 1.65 \frac{m_{\text{smp}} w_E\ \theta_{i_E} N_A \sigma_{\text{tot}}(E_{\text{res}})}{M\ \pi\ r\ (r+h)} \sqrt{\frac{\Gamma_\gamma}{\Gamma_\gamma+\Gamma_n}}$, with $\sigma_{\text{tot}}(E_{\text{res}})$ the resonance neutron cross section of the target isotope, $\Gamma_\gamma$ and $\Gamma_n$ the radiative and neutron resonance widths of the target isotope, respectively. Values of $\sigma_{\text{tot}}(E_{\text{res}})$, $\Gamma_\gamma$ and $\Gamma_n$ are reported in [14] for $^{197}$Au, $^{59}$Co, $^{63}$Cu, $^{115}$In, $^{55}$Mn and $^{183}$Re. For the remaining target isotopes, $\sigma_{\text{tot}}(E_{\text{res}})$ can be worked out form tabulated data of total neutron cross sections available in [15] while updated values of $\Gamma_\gamma$ and $\Gamma_n$ are reported in [16,17];

$$Q_0(\alpha) = \frac{Q_0 - 0.429}{\bar{E}_{\text{r}}^{\alpha}} + \frac{0.429}{0.55^{\alpha}\ (1+2\alpha)} \tag{11}$$

is obtained from the ratio of the resonance integral (for a $1/E$ neutron spectrum in the *epi*-cadmium energy region) to the thermal cross section, $Q_0$, and effective resonance energy $\bar{E}_r$, reported in [18];

$$k_{\varepsilon\Delta d} = e^{\sum_{i=1}^{6} (b_i - b_i^{'}) E^{2-i}} \tag{12}$$

is obtained from fitting parameters $b_i$ and $b_i^{'}$ following the characterization of the γ-ray detection system carried out at nominal counting positions with a set of reference sources covering a suitable energy range;

$$k_{\text{pos}} = \left(\frac{d_{\text{std}} - d_{0\ \text{std}}^{'}}{d_{\text{std}} + \delta d_{\text{std}} - d_{0\ \text{std}}^{'}}\right)^2 \left(\frac{d_{\text{smp}} - d_{0\ \text{smp}}^{'}}{d_{\text{smp}} + \delta d_{\text{smp}} - d_{0\ \text{smp}}^{'}}\right)^{-2} \tag{13}$$

is obtained from the distance between the nominal counting position and the detector end-cap, $d$, the distance between the point-of-action within the detector crystal and the detector end-cap, $d_0^{'}$, and the (small) distance difference between the actual counting position and its nominal counting position, $\delta d$ (see Fig. 2). The methodology adopted to obtain $d_0^{'}$ is described in [6]. The actual counting position is defined at the bottom surface of the sample (the Cartesian coordinate axis originates at detector end-cap and is oriented upwards);

$$k_{\text{geo}} = \left(1 + \frac{h_{\text{std}}}{d_{\text{std}} + \delta d_{\text{std}} - d_{0\ \text{std}}^{'}}\right)^{-1} \left(1 + \frac{h_{\text{smp}}}{d_{\text{smp}} + \delta d_{\text{smp}} - d_{0\ \text{smp}}^{'}}\right) \tag{14}$$

is obtained from $d$, $d_0^{'}$, $\delta d$ and the height of the cylindrical sample, $h$;

$$k_{\text{sa}} = \left(\frac{1 - e^{-\nu_{\text{std}}\ h_{\text{std}}\ \rho_{\text{std}}}}{\nu_{\text{std}}\ h_{\text{std}}\ \rho_{\text{std}}}\right) \left(\frac{1 - e^{-\nu_{\text{smp}}\ h_{\text{smp}}\ \rho_{\text{smp}}}}{\nu_{\text{smp}}\ h_{\text{smp}}\ \rho_{\text{smp}}}\right)^{-1} \tag{15}$$

is obtained from $h$, mass attenuation coefficient, $\nu$, and $\rho$ of the sample, according to the γ-ray self-absorption modelling proposed by Debertin et al. [19] occurring in a cylindrical sample with height $h$ and consisting of a number of elements $E_j$ with mass fraction $w_{E_j}$ and mass attenuation coefficient $\nu_{E_j}$. Specifically, $\nu = \sum_j w_{E_j} \nu_{E_j}$; values for $\nu_{E_j}$ are reported in [20].

It is worth noting that the uncertainty reaches the ultimate minimum when measurement and standard samples are counted at the same nominal counting position. Accordingly, $d_{\text{std}} = d_{\text{smp}} = d$, $d_{0\ \text{std}}^{'} = d_{0\ \text{smp}}^{'} = d_0^{'}$ and $b_i = b_i^{'}$. Eqs. (12), (13) and (14) simplify to

$$\begin{aligned} k_{\varepsilon\Delta d} &= 1 \\ k_{\text{pos}} &= \left(\frac{1 + \frac{\delta d_{\text{smp}}}{d - d_0^{'}}}{1 + \frac{\delta d_{\text{std}}}{d - d_0^{'}}}\right)^2 \\ k_{\text{geo}} &= \left(\frac{1 + \frac{\delta d_{\text{std}}}{d - d_0^{'}}}{1 + \frac{\delta d_{\text{smp}}}{d - d_0^{'}}}\right) \left(\frac{1 + \frac{\delta d_{\text{smp}} + h_{\text{smp}}}{d - d_0^{'}}}{1 + \frac{\delta d_{\text{std}} + h_{\text{std}}}{d - d_0^{'}}}\right) \end{aligned} \tag{16}$$

Additionally, $COI_{\text{std}} = COI_{\text{smp}}$ since the same γ-ray is counted at the same position. As a result, following further simplifications, the measurement equation for the rel-INAA method (5) becomes

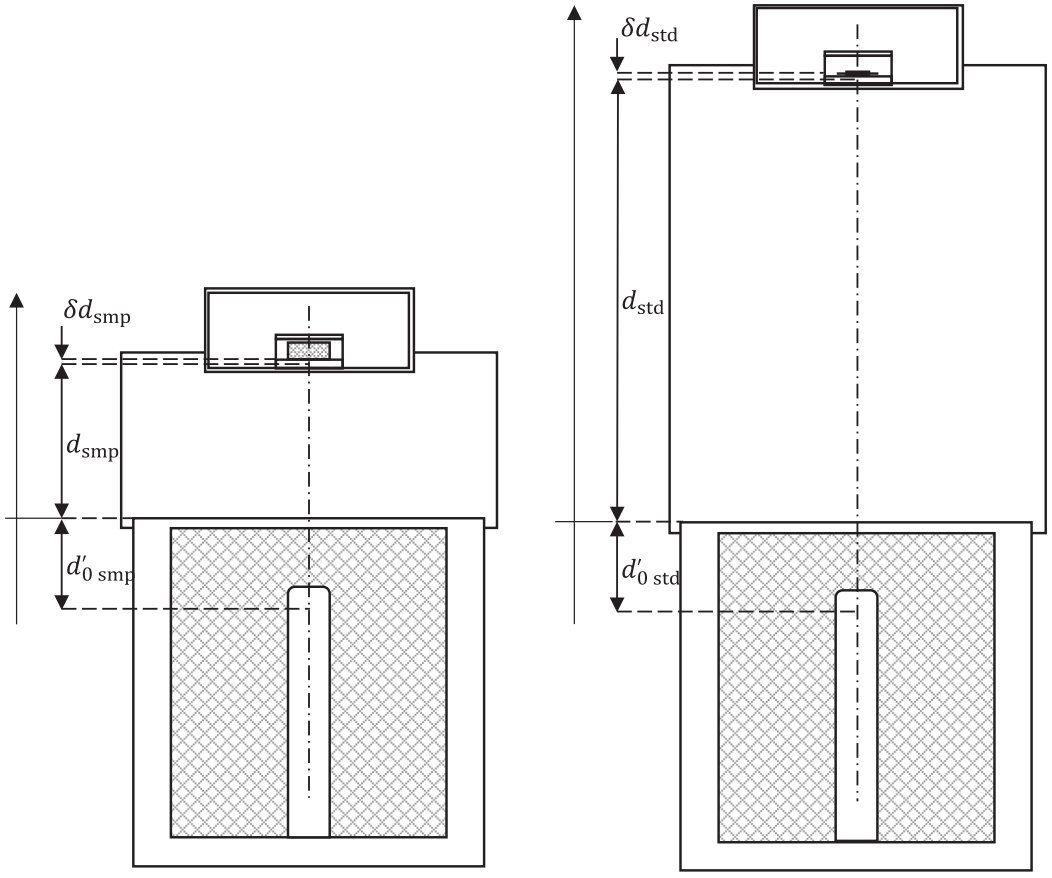


**Fig. 2.** Position of the measurement sample (smp), left-hand side, and standard sample (std), right-hand side, with respect to the detector end-cap and HPGe crystal (indicated by the mesh).

$$
\begin{aligned}
w_{\mathrm{smp}} = & \left( \frac{n_{\mathrm{p\ smp}}}{n_{\mathrm{p\ std}}} \frac{t_{\mathrm{c\ smp}}}{t_{\mathrm{c\ std}}} \frac{t_{\mathrm{l\ std}}}{t_{\mathrm{l\ smp}}} \frac{1 - e^{-\lambda\ t_{\mathrm{c\ std}}}}{1 - e^{-\lambda\ t_{\mathrm{c\ smp}}}} e^{\mu \left( \frac{t_{\mathrm{l\ std}}}{t_{\mathrm{c\ std}}} - \frac{t_{\mathrm{l\ smp}}}{t_{\mathrm{c\ smp}}} \right)} e^{\lambda\ \Delta t_{\mathrm{d}}} \frac{1}{k_{\beta}} \right. \\
& \times \frac{\theta_{i_E\ \mathrm{std}}\ M_{\mathrm{smp}}}{\theta_{i_E\ \mathrm{sm}}\ M_{\mathrm{std}}} \frac{G_{\mathrm{th\ std}} + \frac{G_{\mathrm{e\ std}}}{f}\ Q_0(\alpha)}{G_{\mathrm{th\ smp}} + \frac{G_{\mathrm{e\ smp}}}{f}\ Q_0(\alpha)} \\
& \times \left( \frac{1 + \frac{\delta d_{\mathrm{smp}}}{d - d'_0}}{1 + \frac{\delta d_{\mathrm{std}}}{d - d'_0}} \right) \left( \frac{1 + \frac{\delta d_{\mathrm{smp}} + h_{\mathrm{smp}}}{d - d'_0}}{1 + \frac{\delta d_{\mathrm{std}} + h_{\mathrm{std}}}{d - d'_0}} \right) \\
& \times \left( \frac{1 - e^{-\nu_{\mathrm{std}}\ h_{\mathrm{std}}\ \rho_{\mathrm{std}}}}{\nu_{\mathrm{std}}\ h_{\mathrm{std}}\ \rho_{\mathrm{std}}} \right) \left( \frac{1 - e^{-\nu_{\mathrm{smp}}\ h_{\mathrm{smp}}\ \rho_{\mathrm{smp}}}}{\nu_{\mathrm{smp}}\ h_{\mathrm{smp}}\ \rho_{\mathrm{smp}}} \right)^{-1} \\
& \left. \times\ m_{\mathrm{std}}\ k_{\mathrm{buy}}\ (1 - \eta_{\mathrm{std}})\ w_{\mathrm{std}} - m_{\mathrm{blk}}\ w_{\mathrm{blk}} \right) \frac{1}{m_{\mathrm{smp}} (1 - \eta_{\mathrm{smp}})} - \Delta w_{\mathrm{U}}
\end{aligned}
\tag{17}
$$

The corresponding measurement equation when measurement and standard samples are counted in different nominal counting positions is reported in Appendix A.

## 3. Experimental

The developed measurement Eq. (17) was used to measure the mass fraction of As in a seafood matrix (freeze-dried shrimp powder) within the framework of the APMP.QM-S19 supplementary comparison organized by the Government Laboratory, Hong Kong, China (GLHK).

The neutron activation analysis was carried out using $^{75}$As as the target isotope to produce $^{76}$As ($t_{1/2}$ = 26.2 h) via (n,$\gamma$) reaction. Nine measurement samples of the shrimp powder, about 550 mg mass each, were taken from the bottle provided for the comparison and pressed by a manual hydraulic press to obtain cylindrical tablets with 10 mm diameter and 6.5 mm height. After inspection for visible cracks, tablets were placed in cleaned polyethylene irradiation vials and weighted on a calibrated analytical balance. Barometric pressure, temperature and relative humidity were recorded to calculate the buoyancy correction factor. An additional shrimp powder sample was pressed into a tablet with the same procedure and its height was measured by a caliper and adopted for all the tablets.

The moisture mass to sample mass ratio was evaluated at the same time of tableting by weighing and drying 3 additional shrimp powder samples, 1 g mass each, in a desiccator (anhydrous calcium sulphate) for more than 10 days. The dry mass was calculated by applying a correction to deal with the moisture gained back while the shrimp powder sample was lying on the balance plate during mass measurement.

A mono-elemental As solution with SI traceable 10 mg g$^{-1}$ mass fraction (NIST SRM 3103a) was diluted 1:10 and used to prepare 12 standard samples. A 30 μL volume of the diluted solution was pipetted on a 6 mm diameter absorbent paper disk previously attached to a 10 mm diameter polyethylene adhesive tape disk. The pipetting process was gravimetrically performed on the analytical balance. The mass of the pipetted solution was calculated by applying a correction to deal with the evaporation while the standard was lying on the balance during

mass measurement. Before sealing the standard with a second 10 mm diameter polyethylene adhesive tape disk, the solution was completely evaporated under a fume hood.

Measurement and standard samples were distributed in 3 polyethylene irradiation containers, 3 measurement samples and 4 standard samples each, as represented in Fig. 1. The height of the irradiation vial holding the measurement sample was measured by a caliper and taken as distance between the two standard samples bracketing the measurement sample while the distance between center of mass of the measurement sample and the bottom standard sample is calculated from dimensions of the irradiation vial and measurement sample height.

The neutron irradiation was performed in the TRIGA Mark II reactor of the University of Pavia. The polyethylene irradiation containers were placed in cartridge cases and sent to different channels of the Lazy Susan facility. The neutron exposure lasted 6 h at the maximum 250 kW power.

Measurement and standard samples were extracted from their cartridge cases on the second day after the end of irradiation and placed in γ-counting containers. Measurement samples were left in their irradiation vials while standard disks were inserted in polyethylene vials identical to those of the measurement samples. Gamma spectrometry was performed with a HPGe detector (ORTEC GEM50P4–83, United States, 50% relative efficiency, 1.9 keV full-width half maximum at 1332.5 keV energy) extensively characterized in terms of channel energy and efficiency using a mix of single nuclide γ-sources with SI traceable activities. All measurement and standard samples were counted twice, the first at 80 mm nominal counting position and the second at 40 mm. The acquisitions were performed at fixed real counting time, ranging from 30 min to 70 min, in order to complete the γ-counting of the whole series of samples and standards within a single work day.

Collected γ-spectra of measurement and standard samples were elaborated with HyperLab 2014 software (HyperLabs Software, Hungary) to obtain the number of counts in the 559.1 keV full-energy γ-peak emitted by $^{76}$As (Fig. 3).

Elaborated data were processed using the homemade developed RelINRIM software, implementing the measurement Eq. (17) to produce uncertainty budgets of elemental mass fraction based on the Kragten spreadsheet approach [21], in full agreement with the ISO GUM recommendations [22]. The output uncertainty budgets are compiled in stand-alone and user-adjustable spreadsheets on an individual measurement sample basis using a single γ-spectrum and a single energy emission of the produced radionuclide. Uncertainty budgets on an individual measurement sample basis using multiple γ-spectra and multiple energy emissions can be obtained by suitably combining the compiled uncertainty budgets. The uncertainty budget for the total average mass fraction of different samples is finally calculated by the latter.

**Table 1**
Symbols, modelling equations and names adopted for correction factors, and observed percentage errors.

| Symbol | Equation | Correction factor | Perc. error / % |
|---|---|---|---|
| $k_{f,G}$ | $\frac{G_{\text{th std}} + \frac{G_{\text{e std}}}{f} Q_0(\alpha)}{G_{\text{th smp}} + \frac{G_{\text{e smp}}}{f} Q_0(\alpha)}$ | Neutron energy spectrum and self-shielding | −0.03% |
| $k_\beta$ | $\frac{1}{1+\beta\Delta l}$ | Flux gradient | −1.1% |
| $k_\nu$ | $\left(\frac{1-e^{-\nu_{\text{std}}\, h_{\text{std}}\, \rho_{\text{std}}}}{\nu_{\text{std}}\, h_{\text{std}}\, \rho_{\text{std}}}\right)\left(\frac{1-e^{-\nu_{\text{smp}}\, h_{\text{smp}}\, \rho_{\text{smp}}}}{\nu_{\text{smp}}\, h_{\text{smp}}\, \rho_{\text{smp}}}\right)^{-1}$ | γ-ray self-absorption | −0.6% |
| $k_d$ | $\left(\frac{1+\frac{\delta d_{\text{smp}}}{d-d_0'}}{1+\frac{\delta d_{\text{std}}}{d-d_0'}}\right)\left(\frac{1+\frac{\delta d_{\text{smp}}+h_{\text{smp}}}{d-d_0'}}{1+\frac{\delta d_{\text{std}}+h_{\text{std}}}{d-d_0'}}\right)$ | Counting position and geometry | −5.3%*<br>−8.0%** |
| $k_\eta$ | $\frac{1-\eta_{\text{std}}}{1-\eta_{\text{smp}}}$ | Moisture | −5.3% |
| $k_{\text{buy}}$ | $\frac{1+\left(\frac{1}{\rho_{\text{std}}}-\frac{1}{\rho_c}\right)\rho_a}{1+\left(\frac{1}{\rho_{\text{smp}}}-\frac{1}{\rho_c}\right)\rho_a}$ | Air buoyancy | −0.01% |

* At 80 mm counting distance.
** At 40 mm counting distance.

## 4. Results and discussion

Eighteen As mass fraction values (two each sample counted at 80 mm and 40 mm nominal distances from the detector end-cap) were obtained and the corresponding uncertainty budgets were compiled. Data analysis showed similar combined uncertainties and comparable contributions of the input quantities among samples. Accordingly, averages can be calculated without the use of weight factors.

The impact of the modelling adopted for neutron energy spectrum and self-shielding, flux gradient, γ-ray self-absorption, counting position and geometry, moisture and air buoyancy is evaluated by identifying the corresponding correction factors within the measurement Eq. (17). Adopted symbols, formulae and percentage error observed in this study in case of non-correction are reported in Table 1.

The most overriding correction is $k_d$ and occurs when the measurement sample is close to the detector; following are $k_\eta$ and $k_d$ (when the measurement sample is far from the detector), $k_\beta$ and $k_\nu$, while $k_{f,G}$ and $k_{\text{buy}}$ are negligible.

Results are plotted in Fig. 4 both for the 80 mm and 40 mm counting distance. The averages of the two mass fraction values obtained at the different distances represent the results on a sample-per-sample basis and are indicated in terms of standard uncertainty intervals by the gray

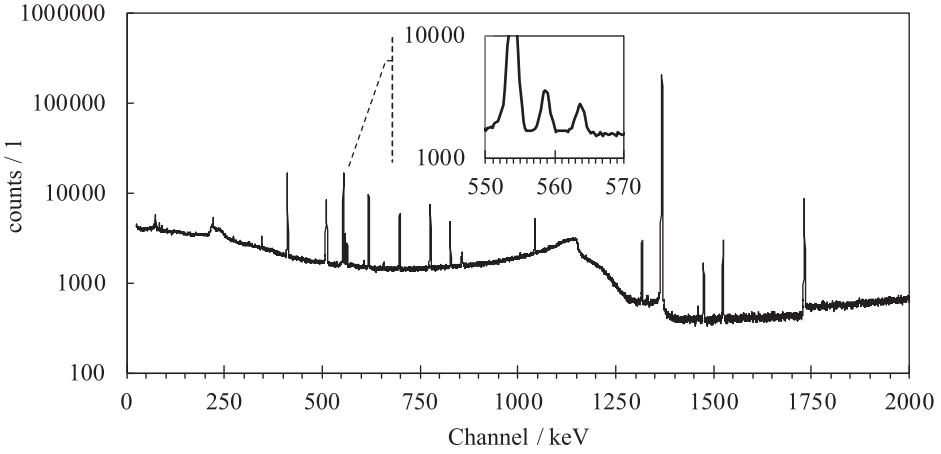


**Fig. 3.** Full γ-spectrum of a measurement sample (shrimp) and zoom of the $^{76}$As peak at 559.1 keV.

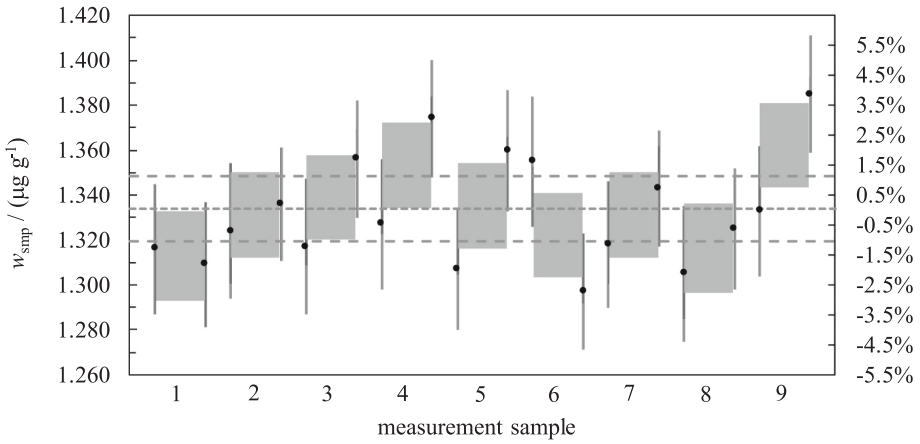


**Fig. 4.** As mass fraction values (left vertical axis) and relative differences from the average (right vertical axis) of 9 shrimp powder samples measured at 80 mm (dots to the left of gray bands) and 40 mm (dots to the right of gray bands) from the detector end-cap. Error bars and gray bands represent standard uncertainties ($k = 1$) of single values and their average (1 sample at two distances), respectively. The center and the upper and lower dashed horizontal lines represent the average (9 samples) and its standard uncertainty ($k = 1$), respectively.

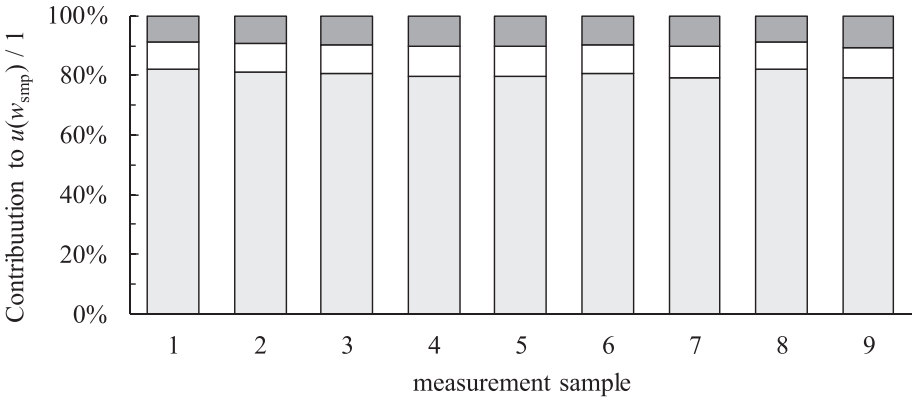


**Fig. 5.** Percentage contribution to the combined uncertainty of As mass fraction on individual sample basis due to counting statistics, $n_{p\ smp}$ and $n_{p\ std}$ (light gray), counting position and geometry, $k_d$ (white), and remaining input quantities (dark gray).

**Table 2**
Result and uncertainty budget of the total average As mass fraction. Input quantities, units, ranges of values of the input quantities, contribution to the uncertainty, degrees of freedom and percentage contributions (Index) to the variance are reported. The expanded uncertainty is calculated at 95% confidence level using the Welch-Satterthwaite formula.

| Quantity | Unit | Range of values | | Uncertainty | DoF | Index |
|---|---|---|---|---|---|---|
| $X$ | $[X_i]$ | min($x_i$) | max($x_i$) | $u_i(y)$ / µg g$^{-1}$ | $\nu_i$ | $I$ / % |
| $n_{p\ smp}$ | 1 | 9010 | 12,100 | 0.0082 | 30 | 30.9 |
| $\lambda$ | s$^{-1}$ | $7.34 \times 10^{-6}$ | $7.34 \times 10^{-6}$ | 0.0065 | 30 | 19.4 |
| $\delta d_{std}$ | mm | 0.4 | 0.4 | 0.0061 | 15 | 17.2 |
| $\delta d_{smp}$ | mm | 0.4 | 0.4 | 0.0059 | 15 | 15.9 |
| $w_{std}$ | µg g$^{-1}$ | 987 | 987 | 0.0040 | 15 | 7.5 |
| $\eta_{smp}$ | 1 | 0.0525 | 0.0525 | 0.0028 | 15 | 3.6 |
| $\beta$ | mm$^{-1}$ | $-2.62 \times 10^{-3}$ | $2.33 \times 10^{-3}$ | 0.0025 | 15 | 2.8 |

| Quantity | Unit | Value | Comb. Unc. | DoF | Exp. Unc. (95%) |
|---|---|---|---|---|---|
| $Y$ | $[Y]$ | $y$ | $u(y)$ | $\nu$ | $U(y)$ |
| $w_{smp}$ | µg g$^{-1}$ | 1.3336 | 0.0148 | 116 | 0.0293 |

bands; the uncertainty budgets highlighted counting statistics and counting position and geometry as the two main contributors, as represented by the histograms plotted in Fig. 5.

Differences of As mass fraction values on a sample-per-sample basis plotted in Fig. 4 are compatible with the combined uncertainties. Accordingly, the uncertainty budget of the total average value is obtained starting from 9 individual sample uncertainty budgets without adding the contribution due to large data scattering. The variance of an input quantity is calculated by averaging the variances of the same input quantity in individual sample uncertainty budgets. Only in case of counting statistics the average variance is divided by the number of samples. The uncertainty budget of the total average As mass fraction value is reported in Table 2; quantities whose percentage contribution to the variance is below 1% have been omitted.

It is worth noting that the uncertainty due to $n_{p\ smp}$ (measurement sample counting statistics) decreased from 0.0246 µg g$^{-1}$ for individual samples to 0.0082 µg g$^{-1}$ for the average of 9 samples. Nevertheless, $n_{p\ smp}$ still represents the most overriding contributor to the combined uncertainty, i.e. 30.9%; following are $\lambda$, $\delta d_{std}$, $\delta d_{smp}$, $w_{std}$, $\eta_{smp}$ and $\beta$.

The results for APMP.QM-S19 supplementary comparison for the determination of As are graphically presented in Fig. 6 [23]; laboratories 1, 16 and 17 have been omitted to zoom on the results closest to the Supplementary Comparison Reference Value (SCRV), estimated by the median of the results included in the calculation. The As result obtained in this study using the rel-INAA method is indicated by INRIM; all other laboratories used secondary standardization methods of Inductively

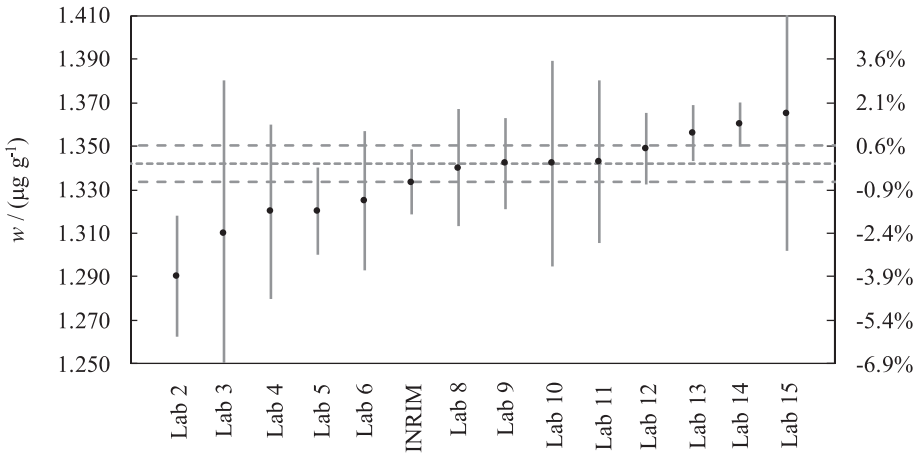


**Fig. 6.** As mass fraction values reported by NMIs/DIs' laboratories in the APMP.QM-S19 supplementary comparison (left vertical axis) and relative differences from the SCRV (right vertical axis). Error bars represent standard uncertainties ($k = 1$). The center and the upper and lower dashed horizontal lines represent the SCRV and its standard uncertainty ($k = 1$), respectively.

Coupled Plasma Mass Spectrometry (ICP-MS), i.e. standard addition (laboratories 2–6, 8–9 and 11–15) and external calibration (laboratory 10).

The absolute degree of equivalence, $d_i$, and its expanded uncertainty at 95% confidence level, $U(d_i)$, calculated for the INRIM result are $-0.008$ µg g$^{-1}$ and 0.034 µg g$^{-1}$, respectively, equivalent to $-0.6$% and 2.5% when expressed as percentages relative to the SCRV [24]. The corresponding $U(d_i)/d_i$ ratio is $-0.25$ and denotes a successful participation in the comparison.

The sum of percentage errors observed in this study if correction factors due to flux gradient, γ-ray self-absorption, counting position and geometry, and moisture are not applied is $-12.3$% or $-$ 15.0%, depending of the nominal counting distance (see Table 2); the adopted modelling is therefore fully validated by the relative degree of equivalence. The same applies to the remaining parts of the measurement Eq. (17) with a significant impact on the result.

## 5. Conclusions

A comprehensive measurement equation for the rel-INAA method was obtained starting from the detailed modelling achieved in the development of the $k_0$-INAA method. It offers the complete mathematical description of the measurand by physical and chemical quantities having dimensions in SI units. In the form presented in this study, the measurement equation is written, to our knowledge for the first time, making the model parameters explicit also for neutron energy spectrum and self-shielding, flux gradient, γ-ray self-absorption, counting position and geometry, moisture and air buoyancy.

This allows claiming metrological traceability to SI of the results obtained by a primary ratio method and based on complete uncertainty budgets automatically compiled using the Kragten spreadsheet approach [21], in full agreement with the ISO GUM recommendation.

The determination of As mass fraction in a seafood matrix within the framework of an international supplementary comparison validated the developed measurement equation to yield results with a performance equivalent to standard addition and external calibration methods of ICP-MS. The added value of the rel-INAA datum is that it was obtained with a method having the potential to be a primary ratio method, with the highest metrological qualities such as isotope dilution of ICP-MS.

In case monoisotopic elements such as Na, Al, Sc, Mn, Co, As, Y, Nb, Rh, I, Cs, Pr, Tb, Ho, Tm, Au and Th, isotopic dilution of ICP-MS is not applicable. This makes rel-INAA the only practically choice as a primary ratio method relevant to the production of certified reference materials for inorganic trace analysis. For the remaining elements, the rel-INAA is also relevant because it does not require prior dissolution of solid samples, a very important feature in the case of particularly complex and heterogeneous matrices, e.g. electronic waste materials.

## CRediT authorship contribution statement

**Giancarlo D'Agostino:** Writing – original draft, Methodology, Funding acquisition, Data curation, Conceptualization. **Marco Di Luzio:** Writing – review & editing, Methodology, Data curation, Conceptualization.

## Declaration of competing interest

The authors have no competing interests to declare that are relevant to the content of this article.

## Data availability

No data was used for the research described in the article.

## Acknowledgements

This project (20IND01 MetroCycleEU) has received funding from the EMPIR programme co-financed by the Participating States and from the European Union's Horizon 2020 research and innovation programme.

## Appendix A

The measurement equation for the rel-INAA method when measurement and standard samples are counted in different nominal counting positions is:

$$w_{\mathrm{smp}} = \left( \frac{n_{\mathrm{p\ smp}}}{n_{\mathrm{p\ std}}} \frac{COI_{\mathrm{std}}}{COI_{\mathrm{smp}}} \frac{t_{\mathrm{c\ smp}}}{t_{\mathrm{c\ std}}} \frac{t_{\mathrm{l\ std}}}{t_{\mathrm{l\ smp}}} \frac{1 - e^{-\lambda\ t_{\mathrm{c\ std}}}}{1 - e^{-\lambda\ t_{\mathrm{c\ smp}}}} e^{\mu \left( \frac{t_{\mathrm{l\ std}}}{t_{\mathrm{c\ std}}} - \frac{t_{\mathrm{l\ smp}}}{t_{\mathrm{c\ smp}}} \right)} e^{\lambda\ \Delta t_{\mathrm{d}}} \frac{1}{k_{\beta}} \right.$$

$$\times \frac{\theta_{i E\ \mathrm{std}}\ M_{\mathrm{smp}}}{\theta_{i E\ \mathrm{smp}}\ M_{\mathrm{std}}} \frac{G_{\mathrm{th\ std}} + \frac{G_{\mathrm{e\ std}}}{f}\ Q_0(\alpha)}{G_{\mathrm{th\ smp}} + \frac{G_{\mathrm{e\ smp}}}{f}\ Q_0(\alpha)}$$

$$\left. \times e^{\sum_{i=1}^{6} \left( b_i - b_i' \right) E^{2-i}} \right. \tag{A1}$$

$$\times \left( \frac{d_{\mathrm{std}} - d'_{0\ \mathrm{std}}}{d_{\mathrm{std}} + \delta d_{\mathrm{std}} - d'_{0\ \mathrm{std}}} \right)^{2} \left( \frac{d_{\mathrm{smp}} - d'_{0\ \mathrm{smp}}}{d_{\mathrm{smp}} + \delta d_{\mathrm{smp}} - d'_{0\ \mathrm{smp}}} \right)^{-2} \left( 1 + \frac{h_{\mathrm{std}}}{d_{\mathrm{std}} + \delta d_{\mathrm{std}} - d'_{0\ \mathrm{std}}} \right)^{-1} \left( 1 + \frac{h_{\mathrm{smp}}}{d_{\mathrm{smp}} + \delta d_{\mathrm{smp}} - d'_{0\ \mathrm{smp}}} \right)$$

$$\times \left( \frac{1 - e^{-\nu_{\mathrm{std}}\ h_{\mathrm{std}}\ \rho_{\mathrm{std}}}}{\nu_{\mathrm{std}}\ h_{\mathrm{std}}\ \rho_{\mathrm{std}}} \right) \left( \frac{1 - e^{-\nu_{\mathrm{smp}}\ h_{\mathrm{smp}}\ \rho_{\mathrm{smp}}}}{\nu_{\mathrm{smp}}\ h_{\mathrm{smp}}\ \rho_{\mathrm{smp}}} \right)^{-1}$$

$$\left. \times\ m_{\mathrm{std}}\ k_{\mathrm{buy}}\ (1 - \eta_{\mathrm{std}})\ w_{\mathrm{std}} - m_{\mathrm{blk}}\ w_{\mathrm{blk}}\ \right) \frac{1}{m_{\mathrm{smp}} (1 - \eta_{\mathrm{smp}})} - \Delta w_{\mathrm{U}}$$

## References


[1] M.J.T. Milton, T.J. Quinn, Primary methods for the measurement of amount of substance, Metrologia 38 (2001) 289–296.

[2] CCQM, Report of the 14th Meeting to the International Committee for Weights and Measures. https://www.bipm.org/en/committees/cc/ccqm/14-2008, 2008 (accessed 24 January 2024).

[3] P. Bode, R.R. Greenberg, E.A. De Nadai Fernandes, Neutron activation analysis: a primary (ratio) method to determine SI-traceable values of element content in complex samples, Chimia 63 (2011) 678–680.

[4] ILAC-G9, Guidelines for the Selection and Use of Reference Materials, 2005.

[5] R.R. Greenberg, P. Bode, E. De Nadai Fernandes, Neutron activation analysis: a primary method of measurement, Spectrochim. Acta B 66 (2011) 193–241.

[6] M. Di Luzio, M.M. Oddone, G. D'Agostino, Developments of the $k_0$-NAA measurement model implemented in k0-INRIM software, J. Radioanal. Nucl. Chem. 331 (2022) 4251–4258, https://doi.org/10.1007/s10967-022-08476-x.

[7] CCQM Working Group on Inorganic Analysis (IAWG), Strategy for 2021-2030. https://www.bipm.org/en/committees/cc/ccqm/wg/ccqm-iawg, 2020 (accessed 24 January 2024).

[8] A. Simonits, F. De Corte, J. Hoste, Single-comparator methods in reactor neutron activation analysis, J. Radioanal. Nucl. Chem. 24 (1975) 31–46.

[9] F. De Corte, The $k_0$-Standardization Method: A Move to the Optimization of Neutron Activation Analysis, 1987. PhD thesis.

[10] G. D'Agostino, M. Di Luzio, M. Oddone, The k0-INRIM software: a tool to compile uncertainty budgets in neutron activation analysis based on $k_0$-standardisation, Meas. Sci. Technol. 31 (2020) 017002, https://doi.org/10.1088/1361-6501/ab358f.

[11] EURAMET, Guidelines on the Calibration of Non-Automatic Weighing Instruments, Calibration Guide n. 18 Version 4.0. https://www.euramet.org/publications-media-centre/calibration-guidelines, 2015 (accessed 24 January 2024).

[12] E. Martinho, J. Salgado, I.F. Gonçalves, Universal curve of the thermal neutron self-shielding factor in foils, wires, spheres and cylinders, J. Radioanal. Nucl. Chem. 261 (2004) 637–643.

[13] V.F. Sears, Neutron scattering lengths and cross sections, Neutron News 3 (3) (1992).

[14] I.F. Gonçalves, E. Martinho, J. Salgado, Extension to cylindrical samples of the universal curve of resonance neutron self-shielding factors, Nucl. Inst. Methods Phys. Res. B 213 (2004) 186–188.

[15] Core Nuclear Reaction Database Maintained by the International Atomic Energy Agency (IAEA). https://www-nds.iaea.org/exfor/endf.htm, 2024 (accessed 24 January 2024).

[16] S.F. Mughabghab, Atlas of Neutron Resonances, Volume 1: Resonance Properties and Thermal Cross Sections Z = 1–60, 6th ed., 2018.

[17] S.F. Mughabghab, Atlas of Neutron Resonances, Volume 1: Resonance Properties and Thermal Cross Sections Z = 61–102, 6th ed., 2018.

[18] $k_0$-Database. https://www.kayzero.com/k0naa/k0naaorg/k0-ISC.html, 2020.

[19] K. Debertin, R.G. Helmer, Gamma- and X-Ray Spectrometry with Semiconductor Detectors, North-Holland, 1988.

[20] J.H. Hubbel, S.M. Seltzer, Tables of X-ray mass attenuation coefficients and mass energy-absorption coefficients from 1 keV to 20 MeV for element Z = 1 to 92 and 48 additional substances of domestic interest, in: NIST Standard Reference Database, 2004, p. 126, https://doi.org/10.18434/T4D01F.

[21] J. Kragten, Calculating standard deviations and confidence intervals with a universally applicable spreadsheet technique, Analyst 119 (1994) 2161–2165.

[22] JCGM 100:2008, Evaluation of Measurement Data – Guide to the Expression of Uncertainty in Measurement, 2008.

[23] K.C. Tse, et al., Supplementary comparison APMP.QM-S19: toxic elements in seafood, Metrologia 61 (2024) 08001.

[24] CCQM, Guidance Note: Estimation of a Consensus KCRV and Associated Degree of Equivalence, Version: 10, 2013-04-12. https://www.bipm.org/, 2013 (accessed 24 January 2024).